Generalized Eddington analytical model for azimuthally dependent radiance simulation in stratified media

Frank S. Marzano and Giancarlo Ferrauto

A fast analytical radiative transfer model to account for propagation of unpolarized monochromatic radiation in random media with a plane-parallel geometry is presented. The model employs an Eddington-like approach combined with the delta phase-function transformation technique. The Eddington approximation is extended in a form that allows us to unfold the azimuthal dependence of the radiance field. A first-order scattering correction to the azimuth-dependent Eddington radiative model solution is also performed to improve the model accuracy for low-scattering media and flexibility with respect to use of explicit arbitrary phase functions. The first-order scattering-corrected solution, called the generalized Eddington radiative model (GERM), is systematically tested against a numerical multistream discrete ordinate model for backscattered radiance at the top of the medium. The typical mean accuracy of the GERM solution is generally better than 10% with a standard deviation of 20% for radiance calculations over a wide range of independent input optical parameters and observation angles. GERM errors are shown to be comparable with the errors due to an input parameter uncertainty of precise numerical models. The proposed model can be applied in a quite arbitrary random medium, and the results are appealing in all cases where speed, accuracy, and/or closed-form solutions are requested. Its potentials, limitations, and further extensions are discussed.

OCIS codes: 290.4210, 280.1310.

1. Introduction

The quantitative evaluation of the electromagnetic (e.m.) radiance field is of major interest for various purposes and applications, as testified in the open literature. The latter go from astrophysics such as the study of the transfer of solar radiation[1–3] to remote sensing such as the retrieval of Earth and planetary atmospheres by passive and active remote sensing techniques[4–7] and to telecommunications such as the effect of Earth's atmosphere on microwave signals.[8–10] In these applications the theory of radiative transfer plays a major role as a suitable model to describe the e.m. interaction and propagation of radiation intensity through a random medium such as a planetary atmosphere and surface.[11–14] In addition to forward modeling, use of fast and fairly accurate radiative transfer solutions can also be essential to solve inverse problems by variational approaches where the solution is searched by minimizing a cost function depending on the measured and simulated radiance observables.[15]

In an absorbing and scattering random medium the radiative transfer equation (RTE) takes the general form of an integrodifferential equation for a monochromatic unpolarized radiance. Its full solution can be accomplished by using several numerical techniques that generally reduce the problem to a set of differential equations in a matrix form with prescribed boundary conditions.[13,16,17,10,9] The interest and the importance in developing analytical approximate solutions of the radiative transfer problem arises from the need to have relatively fast algorithms and from the difficulty to derive precise solutions for many practical applications where the medium properties are not generally known with sufficient accuracy. In this respect, uncertainties in the input parameter description within a given radiative transfer problem tend to reduce the need of calculations with a high degree of precision.[18,19] As already mentioned, the precision of numerical RTE models is obtained at the expense of a long computational time, which is unwanted for applications that require a fast

F. S. Marzano (marzano@die.uniromal.it) is with the Centro di Eccellenza in Telerilevamento E Modellistica di Precipitazioni Severe (CETEMPS), Università dell'Aquila and the Dipartimento di Ingegneria Elettronica, Università La Sapienza di Roma, Via Eudossiana 18, 00184 Roma, Italy. G. Ferrauto is with the Dipartimento di Ingegneria Elettronica, Università La Sapienza di Roma, Via Eudossiana 18, 00184 Roma, Italy.

Received 7 September 2004; accepted 14 February 2005.
0003-6935/05/286032-17$15.00/0

response such as iterative remote sensing techniques.[5,6] (e.g., Kummerow[5]; Tanrè *et al.*[6]).

A number of fast analytical models, with various effective approximations, have been proposed for the solution of the RTE, sacrificing a certain degree of mathematical precision in favor of a closed-form rapid algorithm.[3,12,18–24] The so-called second-order Eddington approximation is probably the most common and effective between these, even though it is generally referred to as the azimuthally averaged form of the RTE for flux calculations.[21,26,27] Azimuthally dependent radiance models represent valuable approximated methods that can yield both irradiance and radiance results.[3,19,28] In particular, these models can be developed in extension of either the two-stream or the Eddington approach[19,20] or are based on the Sobolev approximation framework.[12,28] To maintain consistency between their radiance and irradiance solutions, several approximate solutions need to resort to *ad hoc* numerical integrations so that they could prove unsuitable for applications involving the integration of single RTE solutions over various angular, spectral, and time intervals.

In this paper a fast and fully analytical radiative transfer solution used to calculate the unpolarized monochromatic radiation in a random medium is developed using an Eddington-like approach combined with the delta phase-function transformation technique.[22] In Section 2 the Eddington approximation scheme, proposed by Shettle and Weinman,[21] is extended in a natural way, allowing us to unfold the azimuthal dependence of the radiance field. This approximation, further refined to adequately describe single-scattering phenomena, shows itself sufficiently flexible to be adapted to the treatment of radiation in inhomogeneous random media, schematized through a series of plane-parallel homogeneous adjacent layers. We try to avoid *ad hoc* correction procedures to further improve the overall accuracy; this exercise would reduce the generality of the proposed solution and can always be played for specific applications.[28] In Section 3 results from the generalized Eddington model are then compared over a wide range of optical parameters and observation geometries, with the corresponding solutions generated by a fully numerical and fairly accurate algorithm such as the discrete ordinate radiative transfer (DISORT) method for backscattered radiance at the top of the medium.

2. Generalized Eddington Radiative Model

In this section, we will first introduce the notation of RTE in a rigorous way, then we will illustrate the generalized Eddington model to take into account azimuthal dependence of the radiance field, and finally we will conclude by modifying the analytical solution by means of a first-order scattering correction. The latter choice will also be numerically justified in Section 3.

A. Radiative Transfer Theory

Even though some of the definitions and equations that are given below are quite well known in the literature, we will briefly overview the background concepts with the basic aim to clarify the adopted notation.

The transfer of unpolarized monochromatic radiation in a plane-parallel homogeneous random medium is regulated by the integrodifferential RTE[12–14]:

$$\mu \frac{\mathrm{d}I(\tau,\ \mu,\ \phi)}{\mathrm{d}\tau} = -I(\tau,\ \mu,\ \phi) + J(\tau,\ \mu,\ \phi), \quad (1a)$$

where $I(\tau, \mu, \phi)$ is the diffuse specific intensity (or radiance) along the direction (μ, ϕ) at the optical depth τ and $J(\tau, \mu, \phi)$ is the source function, given by

$$J(\tau,\ \mu,\ \phi) = \frac{\omega}{4\pi}\int_0^{2\pi}\int_{-1}^{1} P(\mu,\ \phi;\ \mu',\ \phi') \times I(\tau,\ \mu',\ \phi')\mathrm{d}\mu'\mathrm{d}\phi' + \frac{\omega}{4\pi} F_0 P(\mu,\ \phi;\ \mu_0,\ \phi_0)\exp(-\tau/\mu_0). \quad (1b)$$

The first term of J is sometimes referred to as the multiple-scattering source, and the second term represents the coherent contribution due to an incident collimated e.m. wave (either a plane wave or a directive beam) along the direction (μ_0, ϕ_0). Thermal emission is assumed to be negligible with respect to the incident beam.[13]

The notation in Eqs. (1a) and (1b) is in accordance with a spherical coordinates system (τ, θ, ϕ), with τ the vertical optical thickness between 0 and τ_s and is as follows (see also Fig. 10 in Appendix B): θ is the zenith (or nadir) angle, $\mu = \cos\theta$ with $\mu > 0$ indicating downward radiance and $\mu < 0$ indicating upward radiance; ϕ is the azimuth angle; ω is the single-scattering volumetric albedo; μ_0 is the cosine of the incident radiation zenith angle θ_0; ϕ_0 is the azimuth angle of the incident radiation; and F_0 is the power flux density, or irradiance, of the incident radiation at $z = 0$. For brevity, the dependence on the wavelength is omitted because, in a way, it is implicitly included in the medium optical parameters τ, ω, and P.

It is worth mentioning that if the incident e.m. source is highly but not infinitively directive, that is, it has a finite field of view such as a pencil beam, Eq. (1a) can be generalized by replacing Eq. (1b) with

$$J(\tau,\ \mu,\ \phi) = \frac{\omega}{4\pi}\int_0^{2\pi}\int_{-1}^{1} P(\mu,\ \phi;\ \mu',\ \phi') \times I(\tau,\ \mu',\ \phi')\mathrm{d}\mu'\mathrm{d}\phi' + \frac{\omega}{4\pi} \times \int_0^{2\pi}\int_{-1}^{1} P(\mu,\ \phi;\ \mu',\ \phi')I_0(\mu',\ \phi') \times \exp(-\tau/\mu_0)\mathrm{d}\mu'\mathrm{d}\phi, \quad (2)$$

where I_0 is the incident radiance field at $z = 0$. If I_0

has a sufficiently narrow beam width, then the second term of Eq. (2) can be approximated by the analogous term in Eq. (1b), as in the case of radar and laser sources. In the same perspective, once the radiance field is computed from Eqs. (1) at a given position, the received power of an antenna (or detector) with a directive gain G can be derived from[10,13]

$$W_r = \frac{\lambda^2}{4\pi}\int_0^{2\pi}\int_{-1}^{1} G(\mu,\ \phi;\ \mu',\ \phi') \times I(\tau,\ \mu',\ \phi')\mathrm{d}\mu'\mathrm{d}\phi', \tag{3}$$

where λ is the e.m. wavelength in the medium.

The zenith opacity at height z can be related to the volumetric extinction coefficient $k_e(z)$ as follows:

$$\tau = \int_0^z k_e(z')\mathrm{d}z', \tag{4}$$

where τ is allowed to vary in the range $[0, \tau_s]$ because τ_s is the total optical depth (see Fig. 10). The irradiance F ($\mathrm{Wm^{-2}\ Hz^{-1}}$) at a given τ is related to radiance through the following integral relationship:

$$F^{\downarrow}(\tau) = \int_0^{2\pi}\int_0^{1} I(\tau,\ \mu',\ \phi')\mathrm{d}\mu'\mathrm{d}\phi',$$

$$F^{\uparrow}(\tau) = \int_0^{2\pi}\int_0^{1} I(\tau,\ -\mu',\ \phi')\mathrm{d}\mu'\mathrm{d}\phi', \tag{5}$$

where $F^{\downarrow}$ and $F^{\uparrow}$ represent the downward and upward fluxes, and from now on we assume μ as a positive quantity (i.e., $\mu = |\cos\theta|$) so that $-\mu$ can be used to designate the upwelling direction. The diffuse upward and downward flux densities, then, are given by Eqs. (5), integrating from 0 and 1 with respect to $-\mu'$ and μ', respectively.

In Eq. (1b), $P(\mu, \phi; \mu', \phi')$ is the so-called volumetric scattering phase function (normalized to 4π), defining the intensity of a radiation incident at direction $\Omega' = (\mu', \phi')$ that is scattered into direction $\Omega = (\mu, \phi)$. In an absorbing and scattering medium with spherical particles, for example, it can be computed by means of Mie theory. The phase function can also be expressed in terms of the scattering angle Θ (i.e., angle between the incident and the scattered radiances). A well-known expansion of the phase function is given by a N-term series of Legendre polynomials P_n (Ref. 13):

$$P(\cos\Theta) = \sum_{n=0}^{N}(2n+1)b_nP_n(\cos\Theta) = \sum_{n=0}^{N}(2n+1)b_nP_n\{\mu\mu' + [(1-\mu^2) \times (1-\mu'^2)]^{1/2}\cos(\phi-\phi')\}, \tag{6}$$

where $P_n(\cos\Theta)$ exhibits orthogonality in a $(-1, 1)$ interval. The coefficients b_n are the moments of P with respect to the polynomials P_n, defined by

$$b_n = \frac{1}{2}\int_{-1}^{1} P(\cos\Theta)P_n(\cos\Theta)\mathrm{d}\cos\Theta, \tag{7}$$

with $P_0(\cos\Theta) = 1$, $P_1(\cos\Theta) = \cos\Theta$ and recursively for higher-order polynomials. Note that $b_0 = 1$ because of the normalization of the phase function, whereas, by definition, b_1, the first moment of the phase function, is called the volumetric asymmetry factor of the phase function.[13,17] This parameter, usually indicated as g, is zero for isotropic scattering and increases as the diffraction peak of the phase function becomes increasingly sharpened. As an example, the Henyey–Greenstein phase function clearly shows more noticeable diffraction peaks associated with higher values of g.[1]

However, Eq. (6) is inadequate to represent strongly asymmetric phase functions. The sharp forward diffraction peaks that characterize phase functions for strongly scattering conditions (i.e., $g > 0.5$) are difficult to reproduce by low-degree polynomials. This implies the need to use higher values of N that would involve an increasing mathematical complexity.[29]

To adequately approximate $P(\cos\Theta)$ with a low number of moments, a delta-function transformation technique can be adopted, introducing a Dirac function describing the sharp peak of the phase function and a series expansion representing the phase function without the peak[18,22]:

$$P(\cos\Theta) \approx P_{\delta}(\cos\Theta) = 2f\delta(1-\cos\Theta) + P^*(\cos\Theta) = 2f\delta(1-\cos\Theta) + \sum_{n=0}^{2M-1}(2n+1)bP_n(\cos\Theta), \tag{8}$$

where f is the fractional scattering into the forward peak. Joseph *et al.*[22] demonstrated that the solution of the RTE (i.e., calculation of the radiance I) using the actual phase function P is equivalent to the solution of the same problem in which P is replaced with the smoothed function P^*, if one set $f = b_{2M}$ and the optical parameters τ, ω, and g are modified as follows:

$$g^* = \frac{g-f}{1-f}, \qquad \omega^* = \frac{1-f}{1-\omega f}\omega, \qquad \tau^* = (1-\omega f)\tau. \tag{9}$$

The advantage in using P^* is related to the fact that its series expansion can be truncated to a small-order Legendre term, since it represents only the smoothed part of the original phase function. It is worth noting that the choice of the peak fraction f is quite arbitrary.

Thus, by use of the delta transformation of the

phase function, analytical complexities of the RTE solution in absorbing and scattering random media, characterized by quite asymmetric phase functions, can be significantly reduced. In Subsections 2.B and 2.C we will always assume that the optical parameters have been transformed by Eqs. (9) with $f = g^2$, derived from imposing the second moment of P equal to that of the Henyey–Greenstein function.[22] For simplicity of notation, later on we will indicate ω^*, g^*, and τ^* by ω, g, and τ, if not otherwise stated.

B. Generalized Solution with an Eddington-Like Approximation

We consider a scattering and absorbing homogeneous random medium with a plane-parallel geometry (i.e., Fig. 10 with $N = 1$). The radiative transfer is governed by Eqs. (1a) and (1b), where all the coefficients are constant. It is clear, however, that a solution for I in a closed form can be derived only under given simplifying approximations.

The generalized Eddington approximation consists of expanding the diffuse radiance in the form of a Fourier cosine series truncated to the first order, that is,

$$I(\tau,\ \mu,\ \phi) = I_0(\tau,\ \mu) + I_1(\tau,\ \mu)\cos\phi, \tag{10a}$$

where the functions $I_0(\tau, \mu)$ and $I_1(\tau, \mu)$ are approximated in accordance with the standard Eddington approach[21]:

$$I_0(\tau,\ \mu) = I_{00}(\tau) + \mu I_{01}(\tau), \tag{10b}$$

$$I_1(\tau,\ \mu) = I_{10}(\tau) + \mu I_{11}(\tau). \tag{10c}$$

The approach, summarized by Eqs. (10), closely resembles the theoretical framework of the discrete ordinate numerical method[30] even though our objective here is to derive a closed-form solution, paying the price of simplifying approximations that will reflect in a less overall accuracy.

From Eqs. (10), the source function J in Eq. (1b) can be rewritten as

$$\begin{aligned} J(\tau,\ \mu,\ \phi) = {} & \omega[I_{00}(\tau) + \mu g I_{01}(\tau)] + \frac{3}{8}\,\pi\omega g(1-\mu^2)^{1/2} \\ & \times I_{10}(\tau)\cos\phi + \frac{\omega}{4\pi} \\ & \times F_0 P(\mu,\ \phi;\ \mu_0,\ \phi_0)\exp(-\tau/\mu_0), \end{aligned} \tag{11}$$

with the phase function approximated by a delta-transformed Sobolev function[12,28]:

$$P = 1 + 3g\cos\Theta. \tag{12}$$

Assuming $\phi_0 = 0$ and integrating Eq. (1a) over ϕ between 0 and 2π, after dividing by 2π, one obtains

$$\begin{aligned} \frac{1}{2\pi}\int_0^{2\pi} \mu\,\frac{\mathrm{d}I(\tau,\ \mu,\ \phi')}{\mathrm{d}\tau}\,\mathrm{d}\phi' &= \mu\,\frac{\mathrm{d}}{\mathrm{d}\tau}\,[I_{00}(\tau) + \mu I_{01}(\tau)] \\ &= -[I_{00}(\tau) + \mu I_{01}(\tau)] + \omega[I_{00}(\tau) + \mu g I_{01}(\tau)] \\ &\quad + \frac{\omega}{4\pi}\,F_0(1 + 3g\mu\mu_0)\exp(-\tau/\mu_0). \end{aligned} \tag{13}$$

Performing the same integration on Eq. (1a) multiplied by $\cos\phi$, we obtain

$$\begin{aligned} \frac{1}{2\pi}\int_0^{2\pi} \mu\,\frac{\mathrm{d}I(\tau,\ \mu,\ \phi')}{\mathrm{d}\tau}\cos\phi'\mathrm{d}\phi' &= \mu\,\frac{\mathrm{d}}{\mathrm{d}\tau}\,[I_{10}(\tau) \\ &\quad + \mu I_{11}(\tau)] \\ &= -[I_{10}(\tau) + \mu I_{11}(\tau)] + \frac{3}{8}\,\omega\pi g(1-\mu^2)^{1/2} I_{10}(\tau) \\ &\quad + \frac{3\omega}{4\pi}\,F_0 g[(1-\mu^2)(1-\mu_0{}^2)]^{1/2}\exp(-\tau/\mu_0). \end{aligned} \tag{14}$$

With the aim to find the solution for $I_{00}(\tau)$ and $I_{01}(\tau)$, it is convenient to integrate Eq. (13) over μ between -1 and 1 and then do the same for Eq. (13) multiplied by μ, obtaining

$$\frac{\mathrm{d}I_{01}(\tau)}{\mathrm{d}\tau} = -3(1-\omega)I_{00}(\tau) + \frac{3\omega}{4\pi}\,F_0\exp(-\tau/\mu_0), \tag{15a}$$

$$\frac{\mathrm{d}I_{00}(\tau)}{\mathrm{d}\tau} = -(1-g\omega)I_{01}(\tau) + \frac{3\omega}{4\pi}\,F_0 g\mu_0\exp(-\tau/\mu_0). \tag{15b}$$

The same procedure, carried out for Eq. (14), yields an analogous system of nonhomogeneous differential linear equations for $I_{10}(\tau)$ and $I_{11}(\tau)$:

$$\begin{aligned} \frac{\mathrm{d}I_{11}(\tau)}{\mathrm{d}\tau} = {} & -3I_{10}(\tau)\left(1 - \frac{3\pi^2}{32}\,\omega g\right) + \frac{9}{16}\,F_0\omega g(1 \\ & - \mu_0{}^2)^{1/2}\exp(-\tau/\mu_0), \end{aligned} \tag{16a}$$

$$\frac{\mathrm{d}I_{10}(\tau)}{\mathrm{d}\tau} = -I_{11}(\tau). \tag{16b}$$

Solutions of the differential equation system, given in Eqs. (15) are

$$\begin{aligned} I_{00}(\tau) = {} & C_{01}\exp(-k_0\tau) + C_{02}\exp(k_0\tau) - \alpha_0 \\ & \times\exp(-\tau/\mu_0), \end{aligned} \tag{17a}$$

$$\begin{aligned} I_{01}(\tau) = {} & p_0[C_{01}\exp(-k_0\tau) - C_{02}\exp(k_0\tau)] - \beta_0 \\ & \times\exp(-\tau/\mu_0), \end{aligned} \tag{17b}$$

where

$$k_0 = [3(1-\omega)(1-g\omega)]^{1/2}, \tag{17c}$$

$$p_0 = \left[\frac{3(1-\omega)}{1-g\omega}\right]^{1/2}, \tag{17d}$$

$$\alpha_0 = \frac{3\omega}{4\pi} F_0 {\mu_0}^2 \frac{I + g(1-\omega)}{1 - {k_0}^2 {\mu_0}^2}, \tag{17e}$$

$$\beta_0 = \frac{3\omega}{4\pi} F_0 \mu_0 \frac{1 + 3g(1-\omega){\mu_0}^2}{1 - {k_0}^2 {\mu_0}^2}. \tag{17f}$$

Analogously, the solution of the differential equation system given by Eqs. (16) is

$$I_{10}(\tau) = p_1[C_{11}\exp(-k_1\tau) - C_{12}\exp(k_1\tau)] - \beta_1 \times \exp(-\tau/\mu_0), \tag{18a}$$

$$I_{11}(\tau) = C_{11}\exp(-k_1\tau) + C_{12}\exp(k_1\tau) - \alpha_1 \times \exp(-\tau/\mu_0), \tag{18b}$$

where

$$k_1 = \left[3\left(1 - \frac{3\pi^2}{32} g\omega\right)\right]^{1/2}, \tag{18c}$$

$$p_1 = \frac{1}{k_1}, \tag{18d}$$

$$\alpha_1 = \frac{(9/16)\omega\mu_0 F_0 g(1-{\mu_0}^2)^{1/2}}{1 - {\mu_0}^2 {k_1}^2}, \tag{18e}$$

$$\beta_1 = \frac{(9/16)\omega\mu_0 F_0 g(1-{\mu_0}^2)^{1/2}}{1 - {\mu_0}^2 {k_1}^2}. \tag{18f}$$

Substituting Eqs. (17) and (18) into Eqs. (10), it is possible to obtain the general solution for azimuth-dependent diffuse radiance, rewritten for clarity in the following way:

$$I(\tau,\ \mu,\ \phi) = I_{00}(\tau) + \mu I_{01}(\tau) + [I_{10}(\tau) + \mu I_{11}(\tau)]\cos\phi. \tag{19}$$

To completely determine the RTE solution, boundary conditions need to be imposed. For a nonreflecting surface, the boundary conditions to compute the integration constants C_{01}, C_{02}, C_{11}, and C_{12} of Eqs. (17) and (18) can be written as

$$I(\tau = 0,\ \mu,\ \phi) = 0, \tag{20a}$$

$$I(\tau = \tau_s,\ -\mu,\ \phi) = 0, \tag{20b}$$

that is, using the generalized Eddington expansion:

$$I_{00}(0) + \mu I_{01}(0) + [I_{10}(0) + \mu I_{11}(0)]\cos\phi = 0, \tag{21a}$$

$$I_{00}(\tau_s) - \mu I_{01}(\tau_s) + [I_{10}(\tau_s) - \mu I_{11}(\tau_s)]\cos\phi = 0. \tag{21b}$$

Trying to determine a solution for the previous system of equations that are valid for all ϕ and for all μ would require us to make equal to zero every term $I_{ij}(0)$ of Eq. (21a) and every term $I_{ij}(\tau_s)$ of Eq. (21b), that is, to solve a system of eight equations with the four unknown constants C_{01}, C_{02}, C_{11}, and C_{12}.

A possible procedure that allows to compute the above-mentioned constants consists of fixing a proper constant value $\mu = \mu_c$ in Eqs. (21). This choice allows us to reduce Eqs. (21) to the following system of four equations with four unknown quantities:

$$\begin{aligned} I_{00}(0) + \mu_c I_{01}(0) &= 0, \\ I_{10}(0) + \mu_c I_{11}(0) &= 0, \\ I_{00}(\tau_s) - \mu_c I_{01}(\tau_s) &= 0, \\ I_{10}(\tau_s) - \mu_c I_{11}(\tau_s) &= 0. \end{aligned} \tag{22}$$

The constant value μ_c can be selected in a manner that, for the azimuthally independent radiance field [i.e., fixing $\cos\phi = 0$ in Eq. (19)], the solution coincides with that obtained adopting the classical Eddington approximation.

To do this, considering that the downward and upward diffuse irradiance, respectively, at the top and the bottom of the medium are zero, it is possible to write from Eqs. (5) the following boundary conditions in terms of downward and upward flux densities (irradiances):

$$\begin{aligned} F^{\downarrow}(0) &= \int_0^{2\pi}\int_0^1 I(0,\ \mu',\ \phi')\mathrm{d}\mu'\mathrm{d}\phi' \\ &= \pi\left[I_{00}(0) + \frac{2}{3} I_{01}(0)\right] = 0, \end{aligned}$$

$$\begin{aligned} F^{\uparrow}(\tau_s) &= \int_0^{2\pi}\int_0^1 I(\tau_s,\ -\mu',\ \phi')\mathrm{d}\mu'\mathrm{d}\phi' \\ &= \pi\left[I_{00}(\tau_s) - \frac{2}{3} I_{01}(\tau_s)\right] = 0, \end{aligned} \tag{23}$$

which suggests that we choose $\mu_c = 2/3$. In Appendix A, a further detailed discussion on this issue from a complementary point of view is provided.

After substituting Eqs. (17) and (18) into Eqs. (22), it is possible to solve the last ones for the unknown constants C_{01}, C_{02}, C_{11}, and C_{12} adopting the value $\mu_c = 2/3$, yielding

$$C_{01}=\frac{\left(\alpha_0-\frac{2}{3}\beta_0\right)\left(1-\frac{2}{3}p_0\right)\exp(-\tau_s/\mu_0)-\left(\alpha_0+\frac{2}{3}\beta_0\right)\left(1+\frac{2}{3}p_0\right)\exp(k_0\tau_s)}{\left(1-\frac{2}{3}p_0\right)^2\exp(-k_0\tau_s)-\left(1+\frac{2}{3}p_0\right)^2\exp(k_0\tau_s)}, \tag{24a}$$

$$C_{02}=\left[\left(\alpha_0+\frac{2}{3}\beta_0\right)-C_{01}\left(1+\frac{2}{3}p_0\right)\right]\frac{1}{\left(1-\frac{2}{3}p_0\right)}, \tag{24b}$$

$$C_{11}=\frac{\left(-\frac{2}{3}\alpha_1+\beta_1\right)\left(-p_1+\frac{2}{3}\right)\exp(-\tau_s/\mu_0)+\left(\frac{2}{3}\alpha_1+\beta_1\right)\left(p_1+\frac{2}{3}\right)\exp(k_1\tau_s)}{-\left(p_1-\frac{2}{3}\right)^2\exp(-k_1\tau_s)+\left(p_1+\frac{2}{3}\right)^2\exp(k_1\tau_s)}, \tag{24c}$$

$$C_{12}=\left[\left(\frac{2}{3}\alpha_1+\beta_1\right)-C_{11}\left(p_1+\frac{2}{3}\right)\right]\frac{1}{\left(-p_1+\frac{2}{3}\right)}. \tag{24d}$$

For several applications, the calculation of the backscattered (or reflected) radiance at the top of the medium is particularly interesting. We call this solution the azimuth-dependent Eddington radiative model (AERM) to distinguish it from that derived in Subsection 2.C. The formal expression of the AERM solution is

$$\begin{aligned} I_{\mathrm{AERM}}(0,\ -\mu,\ \phi) &= I(0,\ -\mu,\ \phi) \\ &= C_{01}+C_{02}-\alpha_0-\mu(p_0C_{01}-p_0C_{02} \\ &\quad -\beta_0)+[p_1C_{11}-p_1C_{12}-\beta_1-\mu(C_{11} \\ &\quad +C_{12}-\alpha_1)]\cos\phi, \end{aligned} \tag{25}$$

where each term on the right-hand side is derived from Eqs. (17), (18), and (24) together with Eqs. (9). As expected, the upwelling irradiance, computed from Eq. (25), is equal to the one given by the classical Eddington approximation:

$$\begin{aligned} F^{\uparrow}(\tau) &= \int_0^{2\pi}\int_0^{-1} I(\tau,\ \mu',\ \phi')\mu'\mathrm{d}\mu'\mathrm{d}\phi' \\ &= \pi[I_{00}(\tau)-(2/3)I_{01}(\tau)], \end{aligned} \tag{26}$$

as found by Shettle and Weinman.[21]

C. First-Order Scattering Correction

The RTE solution for azimuthally dependent radiance, as was shown in Subsection 2.B, is subject to various approximations regarding the form of the phase function and the imposition of the boundary conditions. The truncation of the actual phase function P and its consequential representation with low-order Legendre polynomials allows some essential analytical simplifications, but on the other hand it tends to smooth the angular details of the P behavior and modifies the scattering phenomena description.

By looking at the generalized solution given by Eq. (19) together with Eqs. (24), we realize that the explicit expression of the phase function is no longer traceable. Indeed, from the scattering theory, it is well known that the low orders of radiation scattering, and in particular the single-scattering contribution, are quite sensitive to the approximated representation of P.[3,24,28]

To remove this problem in our theoretical framework, a first-order scattering correction can be carried out. It simply consists of (i) canceling the single-scattering contribution I' (biased by the truncation of the phase function) from the radiance solution I obtained by adopting the Eddington-like scheme of approximation and (ii) replacing I' with I_{FOSM}, the exact weight of the single-scattering effects calculable by the so-called first-order scattering model (FOSM).[14] In Section 3 we will show that this improvement is numerically significant because of this correction.

In the absence of multiple-scattering phenomena, the FOSM represents the exact solution for RTE. For the reflected radiance for a finite homogeneous medium bounded on two sides at $\tau = 0$ and $\tau = \tau_s$, the FOSM solution is given by

$$\begin{aligned} I_{\mathrm{FOSM}}(0,\ -\mu,\ \phi) &= \frac{\omega}{4\pi}\mu_0F_0\frac{P(-\mu,\ \phi;\ \mu_0,\ \phi_0)}{\mu+\mu_0} \\ &\quad \times\left\{1-\exp\left[-\tau_s\left(\frac{1}{\mu}+\frac{1}{\mu_0}\right)\right]\right\}, \end{aligned} \tag{27}$$

where, from now on, I_{FOSM} will be indicated as a first-order scattering (FOS) solution. In the FOS correction scheme, I_{FOSM} is calculated using the actual phase function P and the original optical parameters

τ, g, and ω (i.e., not scaled to account for the delta transformation). Note that only upward backscattered radiance is given here; for the transmitted radiance, similar expressions can be easily derived from an analogous approach.

The single-scattering contribution I' to the generalized solution I, given by Eq. (19), can be computed by removing the multiple-scattering terms within the generalized Eddington model itself. This means that, within the hypothesis of only a single process of scattering, the source function J in Eq. (11) can be approximated by

$$\begin{aligned} J(\tau,\ \mu,\ \phi) &= J_{\mathrm{FOS}}(\tau,\ \mu,\ \phi) \\ &= \frac{\omega}{4\pi} F_0(1 + 3g\{\mu\mu_0 + [(1-\mu^2) \\ &\quad \times (1-\mu_0{}^2)]^{1/2}\cos\phi\})\exp(-\tau/\mu_0). \end{aligned} \tag{28}$$

Repeating the same mathematical steps to obtain the solution for I expressed by Eq. (19), one can simply verify that in this case the general solution for radiance maintains the same form:

$$\begin{aligned} I'(\tau,\ \mu,\ \phi) &= I_{00}'(\tau) + \mu I_{01}'(\tau) \\ &\quad + [I_{10}'(\tau) + \mu I_{11}'(\tau)]\cos\phi, \end{aligned} \tag{29}$$

with

$$I_{00}'(\tau) = C_{01}'\exp(-k_0'\tau) + C_{02}'\exp(k_0'\tau) - \alpha_0' \times \exp(-\tau/\mu_0), \tag{30a}$$

$$I_{01}'(\tau) = p_0'[C_{01}'\exp(-k_0'\tau) - C_{02}'\exp(k_0'\tau)] - \beta_0'\exp(-\tau/\mu_0), \tag{30b}$$

$$I_{10}'(\tau) = p_1'[C_{11}'\exp(-k_1'\tau) - C_{12}'\exp(k_1'\tau)] - \beta_1'\exp(-\tau/\mu_0), \tag{30c}$$

$$I_{11}'(\tau) = C_{11}'\exp(-k_1'\tau) + C_{12}'\exp(k_1'\tau) - \alpha_1' \times \exp(-\tau/\mu_0). \tag{30d}$$

However, for the FOS solution the constants in Eqs. (30a)–(30d) are given by

$$k_0' = \sqrt{3}, \tag{30e}$$

$$p_0' = \sqrt{3}, \tag{30f}$$

$$\alpha_0' = \frac{3\omega}{4\pi} F_0\mu_0{}^2 \frac{1+g}{1-k_0{}'^2\mu_0{}^2}, \tag{30g}$$

$$\beta_0' = \frac{3\omega}{4\pi} F_0\mu_0 \frac{1+3g\mu_0{}^2}{1-k_0{}'^2\mu_0{}^2}, \tag{30h}$$

$$k_1' = \sqrt{3}, \tag{30i}$$

$$p_1' = \frac{1}{k_1'}, \tag{30j}$$

$$\alpha_1' = \frac{\frac{9}{16}\omega\mu_0 F_0 g(1-\mu_0{}^2)^{1/2}}{1-\mu_0{}^2k_1{}'^2}, \tag{30k}$$

$$\beta_1' = \frac{\frac{9}{16}\omega\mu_0{}^2 F_0 g(1-\mu_0{}^2)^{1/2}}{1-\mu_0{}^2k_1{}'^2}. \tag{30l}$$

Moreover, the new constants of integration C_{01}', C_{02}', C_{11}', and C_{12}' are now

$$C_{01}' = \frac{\left(\alpha_0' - \frac{2}{3}\beta_0'\right)\left(1 - \frac{2}{3}p_0'\right)\exp(-\tau_s/\mu_0) - \left(\alpha_0' + \frac{2}{3}\beta_0'\right)\left(1 + \frac{2}{3}p_0'\right)\exp(k_0'\tau_s)}{\left(1 - \frac{2}{3}p_0'\right)^2\exp(-k_0'\tau_s) - \left(1 + \frac{2}{3}p_0'\right)^2\exp(k_0'\tau_s)}, \tag{31a}$$

$$C_{02}' = \left[\left(\alpha_0' + \frac{2}{3}\beta_0'\right) - C_{01}'\left(1 + \frac{2}{3}p_0'\right)\right]\frac{1}{\left(1 - \frac{2}{3}p_0'\right)}, \tag{31b}$$

$$C_{11}' = \frac{\left(-\frac{2}{3}\alpha_1' + \beta_1'\right)\left(-p_1' + \frac{2}{3}\right)\exp(-\tau_s/\mu_0) + \left(\frac{2}{3}\alpha_1' + \beta_1'\right)\left(p_1' + \frac{2}{3}\right)\exp(k_1'\tau_s)}{-\left(p_1' - \frac{2}{3}\right)^2\exp(-k_1'\tau_s) + \left(p_1' + \frac{2}{3}\right)^2\exp(k_1'\tau_s)}, \tag{31c}$$

$$C_{12}' = \left[\left(\frac{2}{3}\alpha_1' + \beta_1'\right) - C_{11}'\left(p_1' + \frac{2}{3}\right)\right]\frac{1}{\left(-p_1' + \frac{2}{3}\right)}. \tag{31d}$$

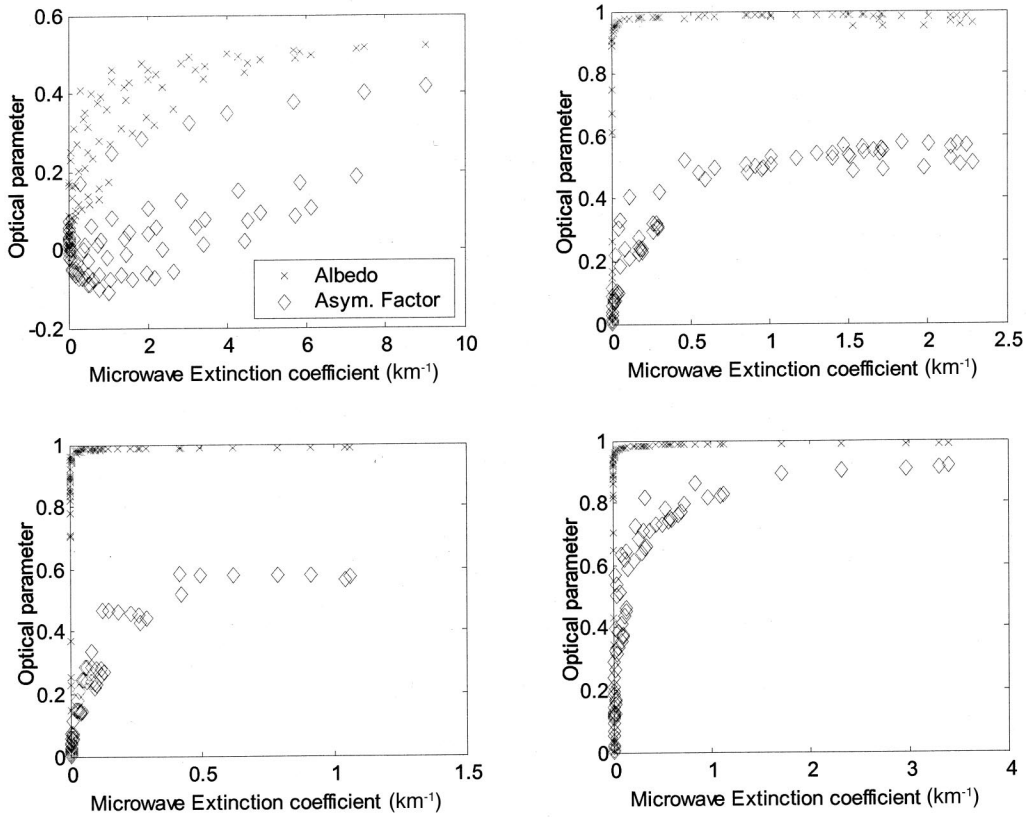

Fig. 1. Optical parameters in terms of albedo and asymmetry factor versus extinction coefficients, as obtained from Mie scattering and absorption simulation for spherical raindrops (upper left panel), graupel particles (upper right panel), ice crystals (bottom left), and snow particles (bottom right) for microwaves between 3 and 90 GHz and a rain rate between 0 and 100 mm/h.

Again, the reflected radiance at the top of the medium is

$$I'(0,\ -\mu,\ \phi) = C_{11}' + C_{02}' - \alpha_0' - \mu(p_0'C_{01}' - p_0'C_{02}' - \beta_0') + [p_1'C_{11}' - p_1'C_{12}' - \beta_1' - \mu(C_{11}' + C_{12}' - \alpha_1')]\cos\phi. \quad (32)$$

In the formulas, the single-scattering correction scheme for simulating the backscattered radiance at the top of the medium can be expressed as

$$I_{\mathrm{GERM}}(0,\ -\mu,\ \phi) = I(0,\ -\mu,\ \phi) - I'(0,\ -\mu,\ \sigma) + I_{\mathrm{FOSM}}(0,\ -\mu,\ \phi), \quad (33)$$

where $I(0, -\mu, \phi)$, $I'(0, -\mu, \phi)$, and $I_{\mathrm{FOSM}}(0, -\mu, \phi)$ are given, respectively, by Eqs. (25), (32), and (27). Equation (33) can be regarded as the closed-form solution of the generalized Eddington radiative model, herein referred to as GERM.

The GERM solution, as well the AERM solution given in Eq. (25), can be simply adapted to the treatment of radiation in inhomogeneous media, schematized through a series of plane-parallel homogeneous adjacent layers, as shown in Appendix B.

3. Numerical Tests

In this section we will show the numerical evaluation of the accuracy of the generalized Eddington model, for both the AERM and the GERM versions, by supposing an arbitrary medium characterized by a large set of optical parameters and observed under several angles.

A. Model Setup

Optical parameters represent the inputs to RTE and their considered variability the domain of the numerical validation test. As an example, Fig. 1 shows the optical parameters in terms of albedo and asymmetry factor as a function of extinction coefficients, as obtained from Mie scattering and absorption simulation for spherical raindrops, graupel particles, ice crystals, and snow particles for microwaves between 3 and 90 GHz and a rain rate between 0 and 100 mm/h.[9,10]

To derive the optical parameters in Fig. 1, an inverse exponential particle size distribution (PSD) has been assumed with the slope parameter parameterized to a surface rain rate. The latter has been derived from the Marshall–Palmer PSD for raindrops, the Sekhon–Srivastava PSD for ice crystals and graupel, and the Gunn–Marshall PSD for snow aggregates.[17] A Gamma PSD has been chosen for cloud droplets. Radius size ranges of cloud droplets, raindrops, ice graupel, ice crystals, and snow have been fixed to 0.001–0.01, 0.1–3.0, 0.1–5, 0.1–1.5, and 0.1–5.0 mm, respectively. Density of ice graupel, ice crystals, and snow has been set to 0.5, 0.2, and

Table 1. Discrete Values Given to the Optical Parameters (albedo ω, asymmetry factor g, and optical thickness τ_s) and Observation Parameters (incident zenith angle θ_0, incident azimuth angle ϕ_0, scattering zenith angle θ, scattering azimuth angle ϕ) Whose Full Combination Defines the Various Test Cases[a]

Parameters							
Optical				Observation			
ω		τ	g	$\mu_0 = \cos\theta_0$	$\mu = \cos\theta$	ϕ (°)	ϕ_0 (°)
0.1	0.91	0.01	0	0.2	0.1	0	0
0.2	0.92	0.03	0.1	0.4	0.2		15
0.3	0.93	0.1	0.2	0.6	0.4		30
0.4	0.94	0.3	0.3	0.8	0.6		60
0.5	0.95	1	0.4	1	0.8		90
0.6	0.96	3	0.5		1		105
0.7	0.97	10	0.6				120
0.8	0.98	30	0.7				150
0.9	0.99	100	0.8				165
		300	0.9				180

[a]The total number of performed tests is equal to 540,000. Note that for the incident wave front it is always assumed that $\phi_0 = 0$.

0.1 g cm^{-3}, respectively. Snow dielectric constant has been derived by a second-order Maxwell–Garnett formula for inclusions of air in an ice matrix. Ambient temperature has been set to 10 °C for cloud droplets and raindrops, 0 °C for ice graupel, and −10° for ice crystals and snow aggregates.

Looking at Fig. 1 and analogous results for visible and infrared radiance in the presence of aerosols and clouds,[6] the variability of input optical parameters of a homogeneous slab has been discretized as shown in Table 1. We have chosen the strategy to stress the approximate solution by letting the optical parameters vary without any physical constraint and correlation. In this respect, we can consider the results below as the worst case in a test scheme. Emphasis will be given to the analysis of backscattered (or reflected) specific intensity at the top of the medium, even though tests on the transmitted specific intensity have also been performed obtaining similar results.

The accuracy of the generalized Eddington solution can arise from the quantitative comparison with RTE numerical solutions, such as the DISORT model.[16] The discrete ordinate model gives highly accurate results in the solution of the RTE so that it is usually considered as a reference.[24,25,28] In the following treatment, then, deviations of the analytical model results from the DISORT solution, obtained with a number M of streams set to 48, are regarded as errors. All simulations are normalized to the incident

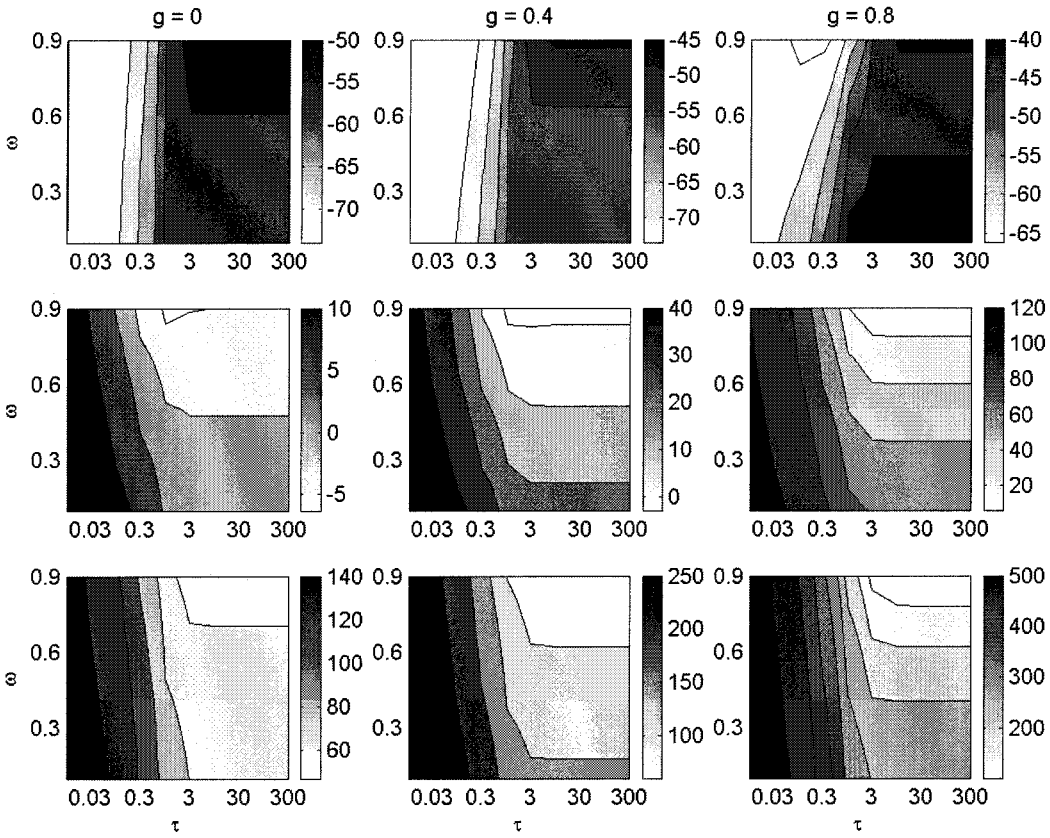

Fig. 2. Accuracy of the AERM solution, given in Eq. (25), illustrated by means of contour plots showing the PFE given in Eq. (34) as a function of optical thickness $\tau = \tau_s$ and albedo ω for asymmetry factor g equal to 0 (right column), 0.4 (middle column), and 0.8 (right column). Incident angles are $\mu_0 = 0.6$ and $\phi_0 = 0°$, and the backscattering (reflection) angles are $\mu = 0.2$ (upper row), $\mu = 0.6$ (middle row), and $\mu = 1.0$ (bottom row) and $\phi = 90°$. Discrete values of τ_s and ω are those prescribed in Table 1.

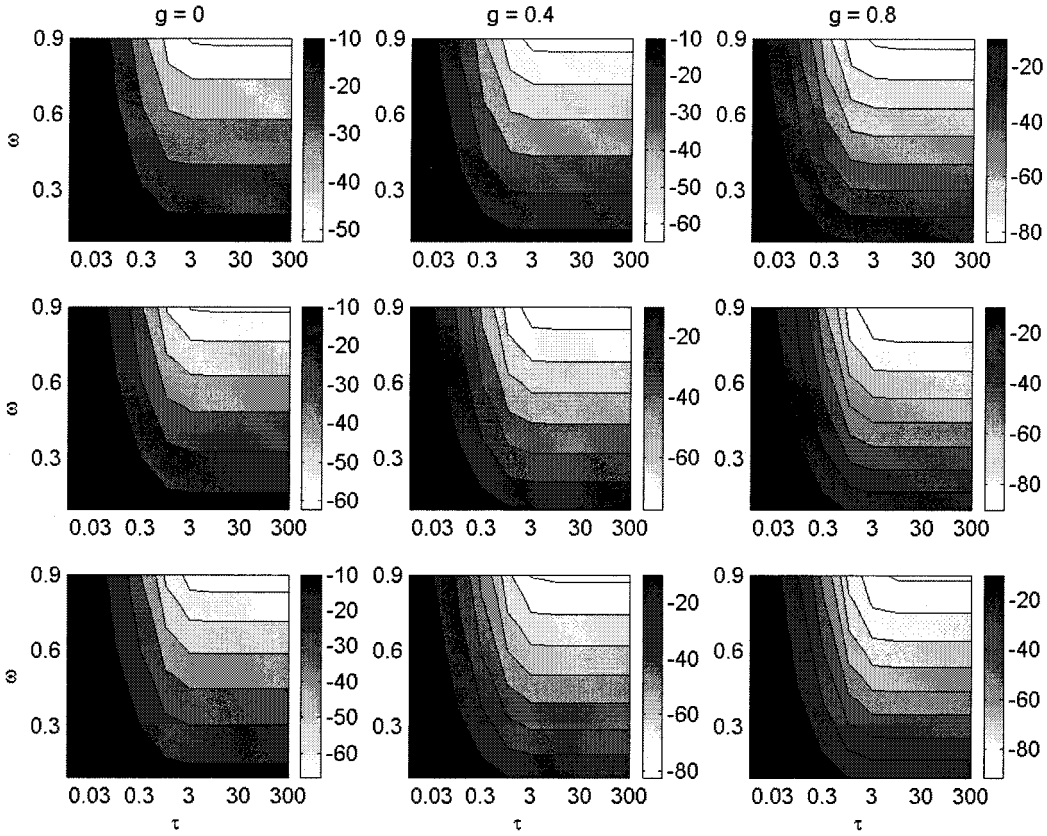

Fig. 3. Same as in Fig. 2, but for the FOSM solution given in Eq. (27) and incident angles $\mu_0 = 0.6$ and $\phi_0 = 0°$.

radiance by setting F_0 equal to 1, whereas ϕ_0 is set to 0 in all tests without loss of generality. A delta-M Henyey–Greenstein phase function, as given in approximation (8), is used for the DISORT phase function.

Differences between the backscattered intensities, calculated by means of each proposed model and the DISORT algorithm, are evaluated for each of the 540,000 test cases of Table 1. These differences are expressed as percentage fractional errors (PFEs) as follows:

$$\varepsilon_f = \frac{I_{\mathrm{GEdd}} - I_{\mathrm{DISORT}}}{I_{\mathrm{DISORT}}} 100, \tag{34}$$

where I_{GEdd} refers to AERM, FOSM, or GERM solutions, and I_{DISORT} refers to the DISORT radiance solution.

B. Numerical Results

To illustrate the various steps of the proposed models, a comparison between AERM and DISORT is first discussed. Figure 2 shows the accuracy of the AERM solution, given by Eq. (25), in terms of contour of the PFE as a function of optical thickness τ_s and albedo ω for asymmetry factor g equal to 0, 0.4, and 0.8. Incident angles are $\mu_0 = 0.6$ and $\phi_0 = 0°$, and the backscattering angles are $\mu = 0.2$, $\mu = 0.6$, and $\mu = 1.0$ and $\phi = 90°$. Discrete values of τ_s, g, and ω are those prescribed in Table 1.

We note that for $\mu = 0.2$ there is a systematic underestimation (up to -65%), which converts to an overestimation for $\mu = 0.6$ (up to 100%) and $\mu = 1.0$ (larger than 300%). AERM also shows a substantial sensitivity to variations of optical parameters g and ω; this model tends to have its greatest accuracy for thick atmospheres and for nearly conservative scattering conditions ($\omega > 0.9$), especially for backscattering zenith angles far from nadir (values of μ much smaller than 1). For brevity, we do not show the results for decreasing values of μ_0, but they confirm the trends commented as above. AERM performs worst in the single-scattering limit, that is, $\tau < 0.1$ (Ref. 23); in these conditions, FOSM is expected to be one of the most accurate among the approximated models.

Therefore, before we illustrate the results relative to the GERM algorithm, Fig. 3 shows the same as in Fig. 2, but for the FOSM solution given in Eq. (27) and with incident angles $\mu_0 = 0.6$ and $\phi_0 = 0°$. The FOSM solution systematically underestimates the DISORT results, even if it exhibits a smaller μ sensitivity than the AERM method. For a given τ and ω, for any μ the percentage error tends to become greater as g increases. Furthermore, FOSM has been confirmed to be a suitable method in the single-scattering limit, especially for scattering conditions far from the conservative case (small values of ω). To a certain extent, FOSM errors exhibit an error trend opposite to that of AERM; it should not be a surprise

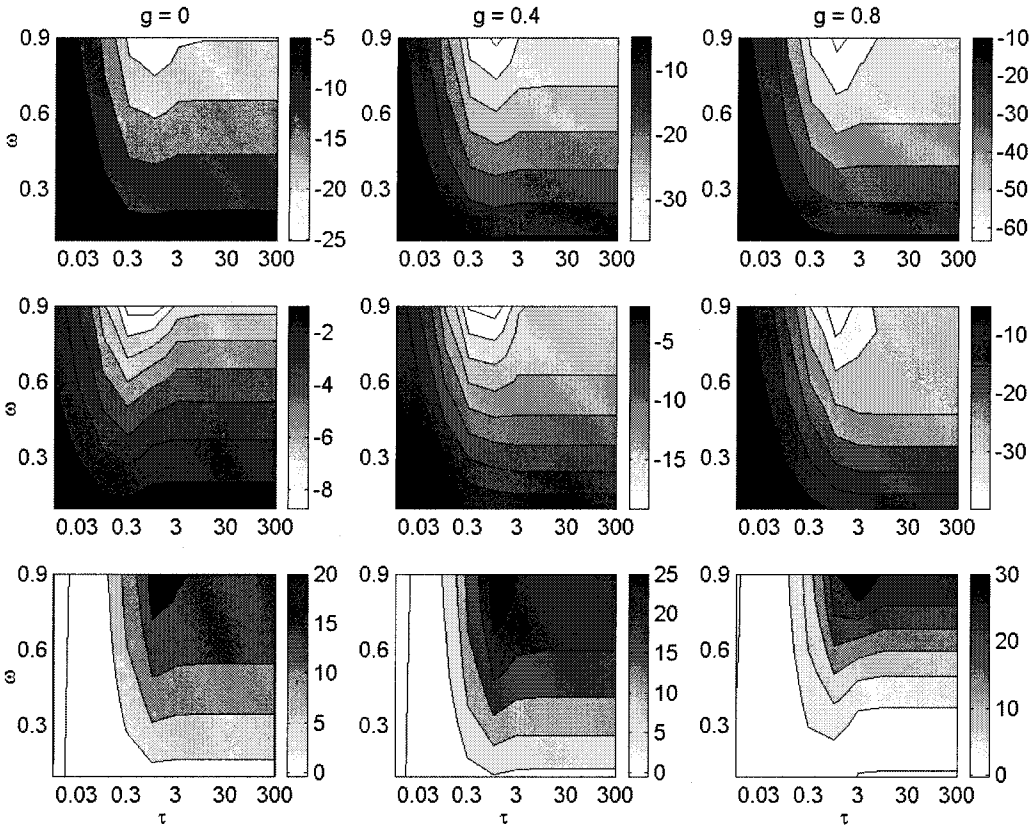

Fig. 4. Same as in Fig. 2, but for the GERM solution given in Eq. (33) and incident angles $\mu_0 = 0.6$ and $\phi_0 = 0°$.

that the combination of the two closed-form solutions can give better results.

Figure 4 shows the same as in Fig. 2, but for the GERM solution given in Eq. (33) and incident angles $\mu_0 = 0.6$ and $\phi_0 = 0°$. To complete the analysis of this intercomparison, Fig. 5 shows the same as in Fig. 4, but for incident angles $\mu_0 = 1.0$ and $\phi_0 = 0°$, and Fig. 6 refers to incident angles $\mu_0 = 0.2$ and $\phi_0 = 0°$. Note that for $\mu_0 = 1.0$ the RTE solution becomes independent from ϕ.

The comparison of Fig. 4 with Figs. 2 and 3 clearly reveals the significant improvement gained by adopting the GERM solution. Maximum error is contained within 25%–30%, except for high albedo ($\omega > 0.8$), small scattering zenith angles ($\mu = 0.2$), and optical depths near unity. The latter behavior is dominated by the AERM solution: It is known from the literature that the Eddington approximation works worst in the neighborhood of optical depth unity.[29] For low scattering conditions, instead, FOSM is predominant. The analysis of Figs. 5 and 6, characterized by $\mu_0 = 1$ and $\mu_0 = 0.2$, respectively, confirms the abovementioned overall error trends for the GERM solution. Furthermore, in the worst conditions (i.e., for $\omega > 0.8$ and τ near unity), Figs. 5 and 6 point out that maximum errors can be found when $\mu = \mu_0$. This result can be explained by noting that, when $\mu \neq \mu_0$, the medium opacity tends to increase so that the diminished transmittance tends to reduce the overall fractional error.

Finally, Fig. 7 illustrates the GERM behavior for extreme values of ω and g and for an intermediate zenith angle ($\mu_0 = 0.6$). In these conditions, classifiable as the worst case from a medium scattering point of view, the GERM accuracy decreases and the PFE grows to values of ~70%. Again, the GERM accuracy becomes particularly worse for values of τ near 1.

The angular dependence of the overall error budget is shown in Fig. 8, where the mean relative error plus and minus its standard deviation band of the PFE are plotted for each zenith cosine angle μ and azimuth angle ϕ, obtained by performing all possible tests prescribed in Table 1 as in Figs. 2–7. From Figs. 2–7 it emerges that the overall mean error is contained within ±20%, with underestimations for μ less than ~0.8 (37°) and overestimations for μ larger than 0.8. The latter behavior can be noted for the azimuth dependence as well for $\phi < 150°$ and $\phi > 150°$, respectively. In both cases the standard deviation of the PFE is ~15%. Analogous figures for the FOSM algorithm (not shown) yield a mean PFE of approximately −30%, and for AERM the mean error ranges from −100% to +100% as the angle increases.

As a summary for the comparison of AERM, FOSM, and GERM, Fig. 9 shows the relative accuracy of these different algorithms in terms of a histogram of the PFE obtained by performing all tests prescribed in Table 1. The overall PFE mean and standard deviation are 10.0% and 152.8% for AERM, −24.1% and 37.9% for FOSM, and −9.4% and 20.1%

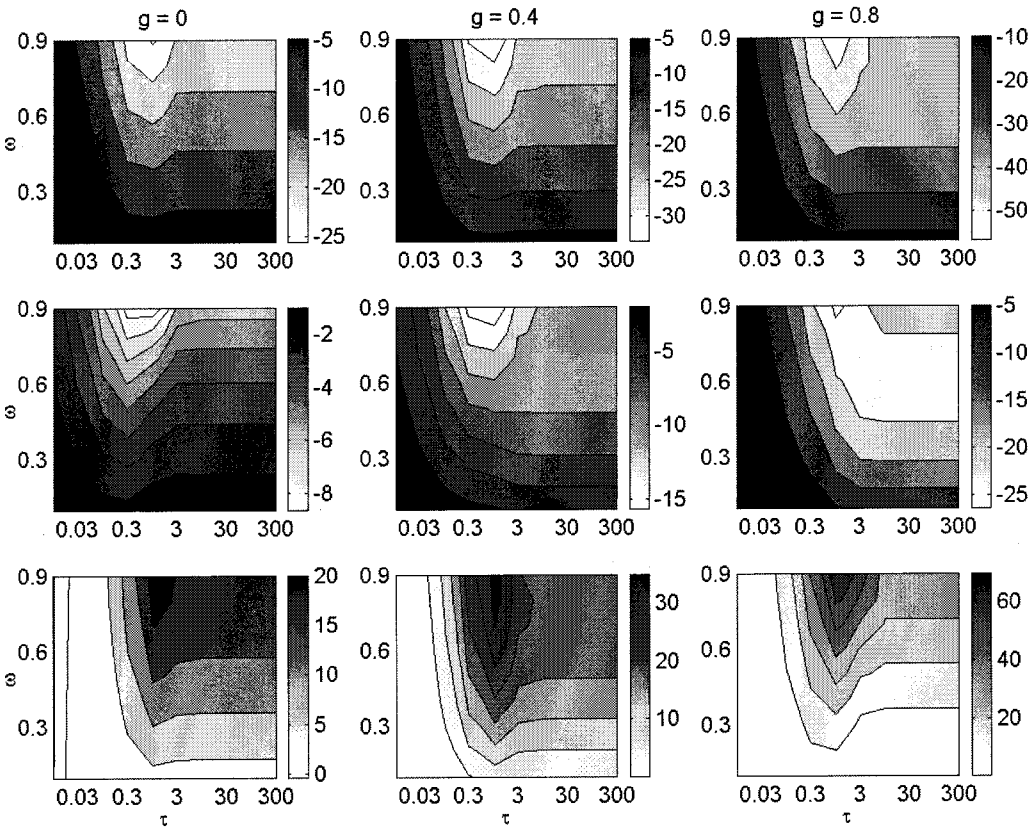

Fig. 5. Same as in Fig. 2, but for the GERM solution given in Eq. (33) and incident angles $\mu_0 = 1.0$ and $\phi_0 = 0°$.

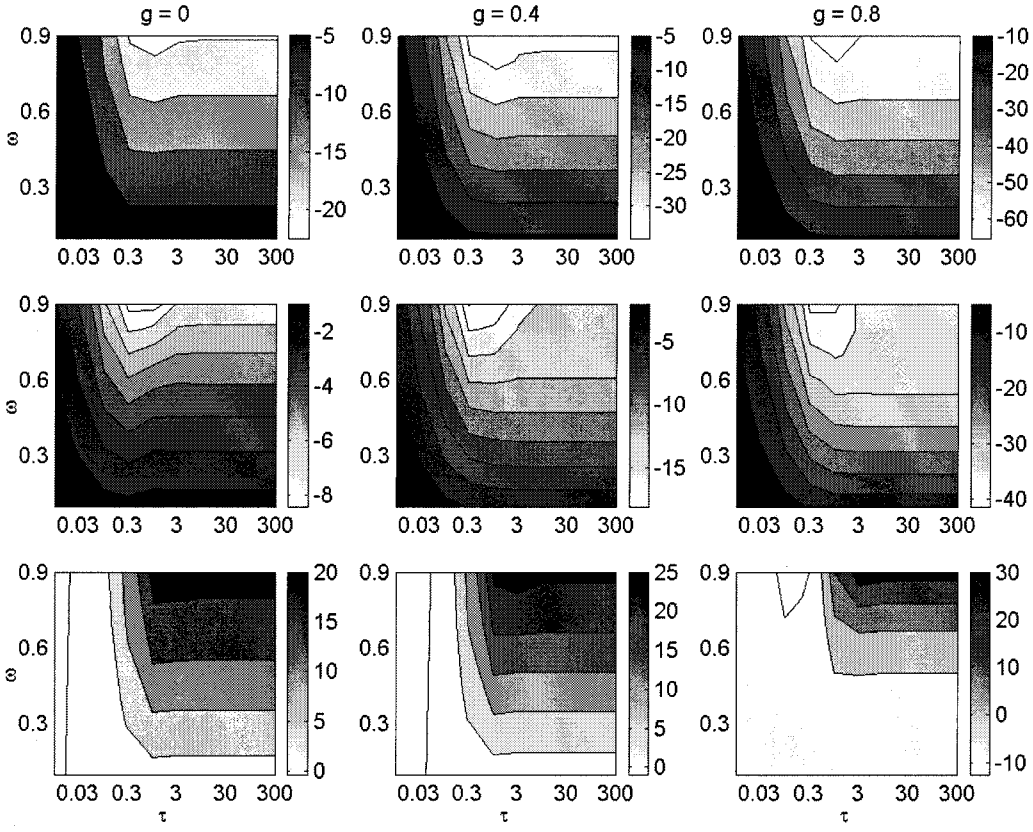

Fig. 6. Same as in Fig. 2, but for the GERM solution given in Eq. (33) and incident angles $\mu_0 = 0.2$ and $\phi_0 = 0°$.

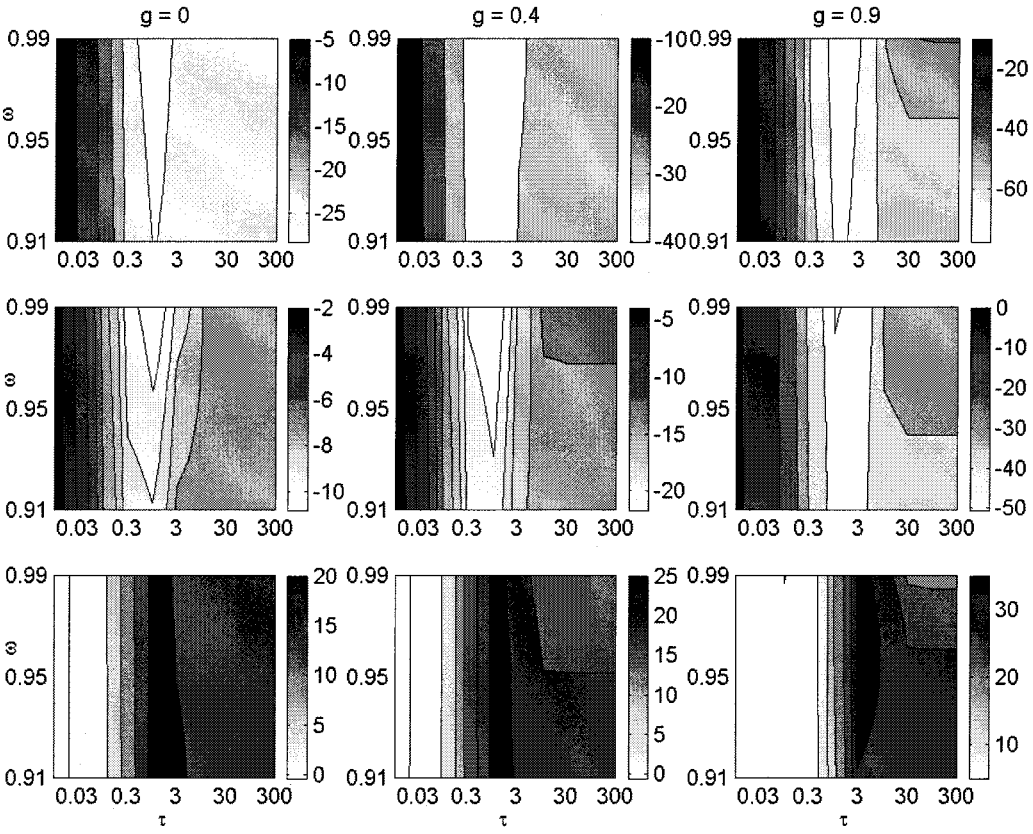

Fig. 7. Same as in Fig. 4 for the GERM solution, but with extreme values of ω and g.

for GERM. If a subset of scattering conditions characterized by ω ranging from 0.1 to 0.9 is considered, leaving unchanged all the other optical parameter values of Table 1 (i.e., 270,000 test cases), the overall PFE mean and standard deviation come down to 7.9% and 16.6% for GERM, respectively.

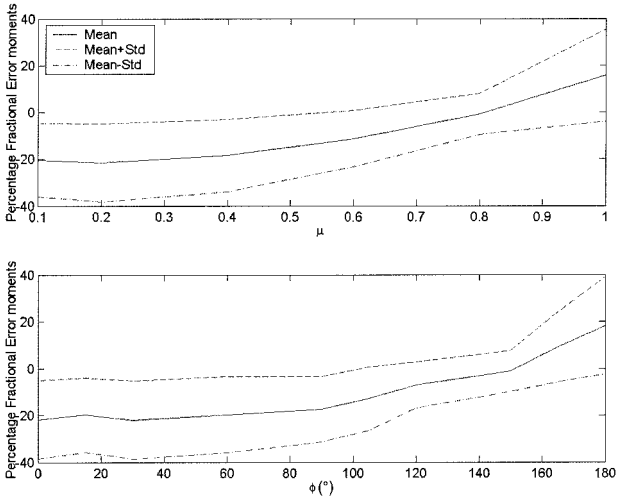

Fig. 8. Top panel: Overall accuracy of the GERM solution in terms of moments of the PFE given in Eq. (34) as a function of azimuth angle μ by performing all tests prescribed in Table 1, derived from all possible combinations of optical parameter discrete values. Mean relative error plus and minus its standard deviation band are plotted for each zenith angle μ. Bottom panel: Same as in top panel, but as a function of azimuth angle ϕ.

Such a level of accuracy in the radiance computation can be considered acceptable for several applications since errors and uncertainties in the measure of the absorbing and scattering properties of the medium can produce comparable errors in the retrieval of the radiance field.[19] Numerical experiments have been carried out by supposing uncertainties in the knowledge of input optical parameters uniformly distributed in the range 0%–10%. The true and the biased intensities have both been calculated by the DISORT model, the biased values being computed using input optical parameters affected by uncertainty. An analysis of the results shows that the standard errors are ~15% due to the nonlinearity of the RTE and thus are substantially comparable with those obtainable from GERM.

As a final comment, it is opportune to remark that the above analysis has been conducted over a wide range of absorbing and scattering conditions of the medium, considering an exhaustive number of observing geometries. Once the particular application requiring the retrieval of the radiance field is specified, a better accuracy can be obtained by restricting the analysis to the corresponding range of optical parameters and viewing geometries. In particular, a tuning of the exponent of the μ_0 term in the numerator of both the α_1 and the β_1 coefficients given by Eqs. (18e) and (18f), in a way similar to that proposed

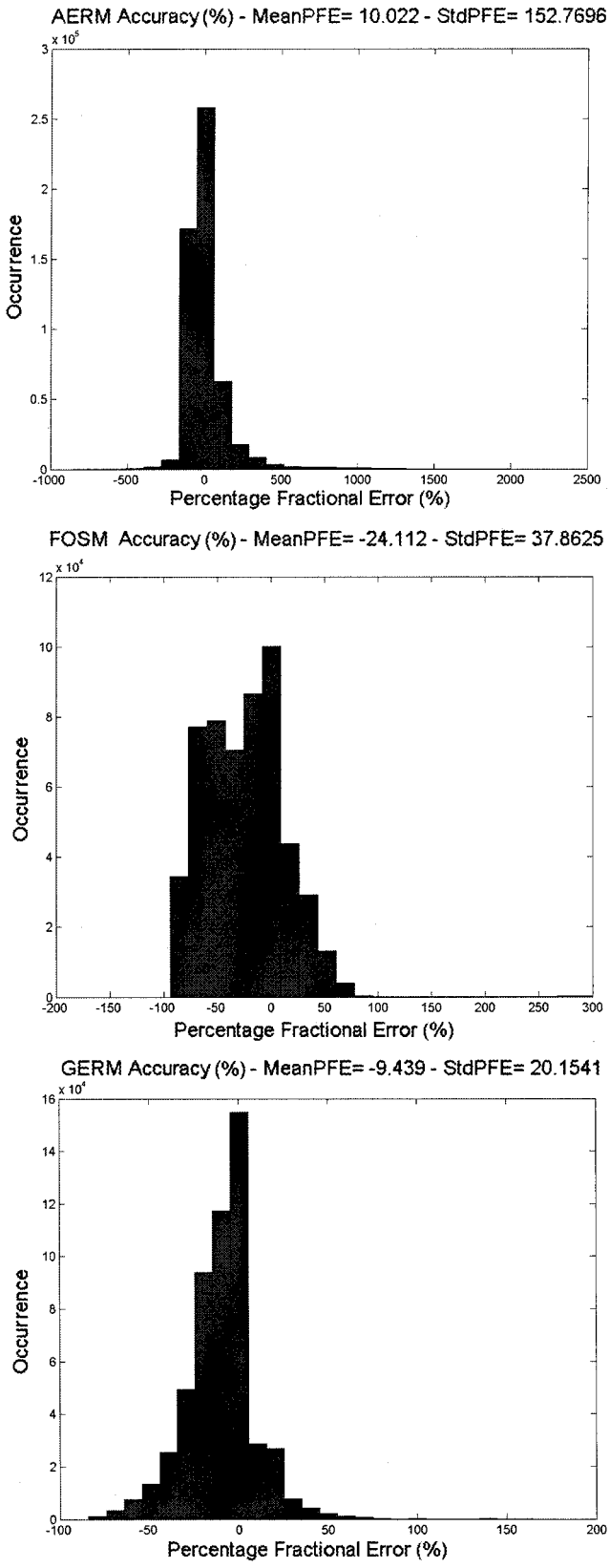

Fig. 9. Comparison of relative accuracy of AERM (top panel), FOSM (middle panel), and GERM (bottom panel) solutions in terms of a histogram of the PFE given in Eq. (34) by performing all tests prescribed in Table 1 from all possible combinations of optical parameter discrete values. Mean relative error and its standard deviation are also indicated.

by Xiang *et al.*,[28] allows us to improve the accuracy for the specified application by halving the obtained error results.[31]

4. Conclusions

A fast analytical approximated method of a solution for the RTE, based on the generalization of the Eddington approximation and capable of unfolding the azimuthal dependence of the radiance field, has been developed in this paper. Performances of this new radiative model, called GERM, in simulating the backscattered (reflected) intensity field due to a plane-parallel homogeneous medium excited by a incident radiation, have been evaluated by comparison with the DISORT model.

The consequences of this approximation used to express the radiance field are mean percentage errors in the intensity calculations less than ~10% with a standard deviation of ~20% over an extremely wide range (540,000 samples) of independent values of single-scattering albedo, asymmetry factor, optical depth, and incident radiation direction. The significance of such errors is less relevant in problems where the input parameters are known with a certain degree of uncertainty. In particular, it has been shown that the related level of accuracy is sufficient when the uncertainties in the knowledge of the optical parameters are uniformly distributed in the range 0%–10%.

The overall accuracy is comparable, if not better, than available azimuthally dependent analytical models such as those by Davies[19] and Xiang *et al.*,[28] based on the Eddington and Sobolev approximations, respectively. A thorough comparison might be possible even though each analytical model tends to use *ad hoc* corrections to improve the numerical accuracy. It is worth mentioning that the results shown in Section 3.B are obtained without any specific tuning of the model parameters. This approach, justified by the need to illustrate results depending as less as possible on arbitrary choices, opens, indeed, a wide possibility in the refinements of GERM for specific applications.[31]

The worse accuracy in reproducing the radiance field, as compared with the DISORT model, is obviously balanced by a more rapid calculation of the radiance itself. In this respect, we note that the computational time of the DISORT model is approximately proportional to N^2, with $2N$ the number of streams, whereas the generalized Eddington model has a constant computational complexity. This feature makes the proposed GERM well suited to problems that require iterations over finite spectral and/or time intervals. Moreover, as mentioned above, for a specific application requiring the computation of the radiance field, a better accuracy can be obtained by restricting the analysis to the corresponding range of optical parameters and viewing geometries.

The main theoretical limitations of GERM are related to the assumption of (i) stratified medium ge-

ometry and (ii) unpolarized radiation. With respect to the first item, the plane-parallel geometry allows us to simplify the general expression of the RTE in a three-dimensional (3-D) space and to unfold the angular dependence of radiance through the generalized Eddington approximation. A way to apply GERM to a 3-D problem is to resort to a one-dimensional (1-D) slant geometry along the viewing angle, that is to construct an equivalent 1-D problem from the given 3-D one.[9,32] The limitation due to the hypothesis of unpolarized radiance can be removed only if the elements of the rotated phase matrix can be approximated by means of a Sobolev phase function as in Eq. (12). The validity of this approximation would, of course, depend on the properties of the particle distribution.

Future work will be devoted to possibly extend GERM to a polarized radiation and to perform a systematic comparison with other numerical solutions such the finite-element method[10] and available analytical approximated models. Application to the remote sensing of the atmosphere is also foreseen, and its tests could be carried out by following an approach similar to that of Smith *et al.*[25]

Appendix A: Boundary Conditions

In Subsection 2.B it was shown that computation of the integration constants C_{00}, C_{01}, C_{10}, and C_{11}, relative to the radiance general solution, is subject to some approximations. In this appendix we point out the proposed approach in an explicit way.

The choice of the above-mentioned approximations can be justified through a direct comparison with those proposed by Xiang *et al.*[28] The latter boundary conditions, expressed in terms of irradiances, assume the following form:

$$\int_0^{2\pi}\int_{-1}^{1} I(0,\ \mu',\ \phi')\mathrm{d}\mu'\mathrm{d}\phi' \approx -2\int_0^{2\pi}\int_{-1}^{1} I(0,\ \mu',\ \phi')\mu'\mathrm{d}\mu'\mathrm{d}\phi', \quad \text{(A1)}$$

$$\int_0^{2\pi}\int_{-1}^{1} I(\tau_s,\ \mu',\ \phi')\mathrm{d}\mu'\mathrm{d}\phi' \approx -2\int_0^{2\pi}\int_{-1}^{1} I(\tau_s,\ \mu',\ \phi')\mu'\mathrm{d}\mu'\mathrm{d}\phi', \quad \text{(A2)}$$

$$\int_0^{2\pi}\int_{-1}^{1} I(0,\ \mu',\ \phi')(1-\mu'^2)^{1/2}\cos\phi'\mathrm{d}\mu'\mathrm{d}\phi' \approx \frac{2}{3}\int_0^{2\pi}\int_{-1}^{1}\left.\frac{\mathrm{d}I(\tau,\ \mu',\ \phi')}{\mathrm{d}\tau}\right|_{\tau=0} \times (1-\mu'^2)\cos\phi'\mathrm{d}\mu'\mathrm{d}\phi', \quad \text{(A3)}$$

$$\int_0^{2\pi}\int_{-1}^{1} I(\tau_s,\ \mu',\ \phi')(1-\mu'^2)^{1/2}\cos\phi'\mathrm{d}\mu'\mathrm{d}\phi' \approx -\frac{2}{3}\int_0^{2\pi}\int_{-1}^{1}\left.\frac{\mathrm{d}I(\tau,\ \mu',\ \phi')}{\mathrm{d}\tau}\right|_{\tau=\tau_s} \times (1-\mu'^2)\cos\phi'\mathrm{d}\mu'\mathrm{d}\phi'. \quad \text{(A4)}$$

These expressions have a general validity, so they can be applied to the generalized Eddington model solution, expressed by Eq. (19).

Thus, substituting into Eqs. (1) the expression of radiance given by Eqs. (10), one obtains

$$\begin{aligned}\int_0^{2\pi}\int_{-1}^{1} &\{[I_{00}(0)+\mu' I_{01}(0)]+[I_{01}(0) + \mu' I_{11}(0)]\cos\phi'\}\mathrm{d}\mu'\mathrm{d}\phi' \\ &\approx -2\int_0^{2\pi}\int_{-1}^{1}\{[I_{00}(0)+\mu' I_{01}(0)]+[I_{10}(0) + \mu' I_{11}(0)]\cos\phi'\}\mu'\mathrm{d}\mu'\mathrm{d}\phi', \end{aligned} \quad \text{(A5)}$$

and then integrating, we obtain

$$I_{00}(0) \approx -\frac{2}{3} I_{01}(0). \quad \text{(A6)}$$

Starting from approximation (A2), with analogous mathematical passages, we obtain

$$I_{00}(\tau_s) \approx \frac{2}{3} I_{01}(\tau_s). \quad \text{(A7)}$$

Inserting now the expression of radiance into approximation (A3), the latter can be rewritten as follows:

$$\int_0^{2\pi}\int_{-1}^{1}[I_{10}(0)+\mu' I_{11}(0)](1-\mu'^2)^{1/2}\cos^2\phi'\mathrm{d}\mu'\mathrm{d}\phi' \approx \frac{2}{3}\int_0^{2\pi}\int_{-1}^{1}\left.\frac{\mathrm{d}I_1(\tau,\ \mu')}{\mathrm{d}\tau}\right|_{\tau=0}(1-\mu'^2)\cos^2\ \phi'\mathrm{d}\mu'\mathrm{d}\phi', \quad \text{(A8)}$$

where the intensity terms, multiplied by cos ϕ, have been omitted for brevity as they cancel when integrated over ϕ.

Considering Eqs. (10c) and (18), it is simple to verify that

$$\frac{\mathrm{d}I_1(\tau,\ \mu)}{\mathrm{d}\tau} = -I_{11}(\tau) + \mu\left[-k_1 C_{11}\exp(-k_1\tau) + k_1 C_{12}\exp(k_1\tau) + \frac{\alpha_1}{\mu_0}\exp(-\tau/\mu_0)\right], \quad \text{(A9)}$$

so that approximation (8) becomes

$$\int_0^{2\pi}\int_{-1}^{1}[I_{10}(0)+I_{11}(0)](1-\mu'^2)^{1/2}\cos^2\phi'\,d\mu'd\phi' \approx \frac{2}{3}\int_0^{2\pi}\int_{-1}^{1}\left[-I_{11}(0)+\mu'\left(k_1C_{11}+k_1C_{12}+\frac{\alpha_1}{\mu_0}\right)\right]\times(1-\mu'^2)^{1/2}\cos^2\phi'\,d\mu'd\phi',$$

that is,

$$I_{10}(0)\approx-\frac{2}{3}I_{11}(0). \tag{A10}$$

In the same way, approximation (4) produces the following relation:

$$I_{10}(\tau_s)\approx\frac{2}{3}I_{11}(\tau_s). \tag{A11}$$

Equations (A6), (A7), (A10), and (A11) are analogous to the approximations expressed by Eqs. (22), adopted in Subsection 2.B for the calculation of the constants C_{01}, C_{02}, C_{11}, and C_{12} and consequently for the computation of the radiance field.

Appendix B: Generalized Solution for Vertically Inhomogeneous Media

Electromagnetic propagation in a vertically inhomogeneous random medium is usually approached by approximating the medium through a series of homogeneous adjacent layers (e.g., Ishimaru,[13] Stamnes *et al.*[30]).

In particular, media can be represented with a number N_l of plane-parallel layers, as shown in Fig. 10. Each layer is characterized by different values of ω_i and g_i, with

$$\frac{d\omega_i}{d\tau}=\frac{dg_i}{d\tau}=0,\qquad i=1,\,2,\,\ldots,\,N. \tag{B1}$$

Thus the solution of the RTE through the generalized Eddington approximation is appropriate within each layer. For the ith layer with optical thickness $\tau_s^{\,i}=\tau_i-\tau_{i-1}$, the RTE allows for the following analytical solution:

$$I^i(\tau,\,\mu,\,\phi)=I_{00}{}^i(\tau)+\mu I_{01}{}^i(\tau)+[I_{10}{}^i(\tau)+\mu I_{11}{}^i(\tau)]\cos\phi,\qquad \tau_{i-1}<\tau<\tau_i, \tag{B2}$$

where $\tau_0=0$ and $\tau_N=\tau_s$, and the general solution is given by

$$I(\tau,\,\mu,\,\phi)=I^i(\tau,\,\mu,\,\phi),\qquad \tau_{i-1}<\tau<\tau_i. \tag{B3}$$

Furthermore, it holds that

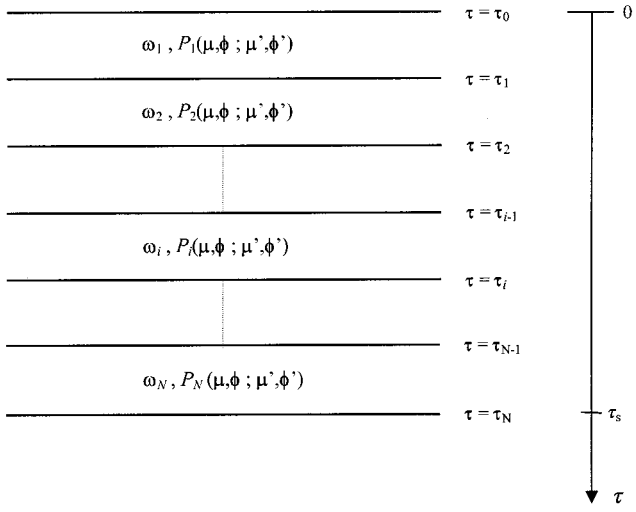

Fig. 10. Representation of an inhomogeneous random medium with a plane-parallel geometry with N homogeneous scattering layers characterized by albedo ω and phase function P.

$$I_{00}{}^i(\tau)=C_{01}{}^i\exp(-k_0{}^i\tau)+C_{02}{}^i\exp(k_0{}^i\tau)=\alpha_0{}^i\exp(-\tau/\mu_0), \tag{B4a}$$

$$I_{01}{}^i(\tau)=p_0{}^i[C_{01}{}^i\exp(-k_0{}^i\tau)+C_{02}{}^i\exp(k_0{}^i\tau)]-\beta_0{}^i\times\exp(-\tau/\mu_0), \tag{B4b}$$

$$I_{11}{}^i(\tau)=C_{11}{}^i\exp(-k_1{}^i\tau)+C_{12}{}^i\exp(k_1{}^i\tau)-\alpha_1{}^i\times\exp(-\tau/\mu_0), \tag{B4c}$$

$$I_{10}{}^i(\tau)=C_{11}{}^i\exp(-k_1{}^i\tau)+C_{12}{}^i\exp(k_1{}^i\tau)-\beta_1{}^i\times\exp(-\tau/\mu_0), \tag{B4d}$$

where

$$k_0{}^i=[3(1-\omega_i)(1-g_i\omega_i)]^{1/2},$$

$$p_0{}^i=[3(1-\omega_i)/(1-g_i\omega_i)]^{1/2},$$

$$\alpha_0{}^i=\frac{3\omega_i}{4\pi}F_0{\mu_0}^2\frac{1+g_i(1-\omega_i)}{1-(k_0{}^i\mu_0)^2},$$

$$\beta_0{}^i=\frac{3\omega_i}{4\pi}F_0\mu_0\frac{1+3g_i(1-\omega_i){\mu_0}^2}{1-(k_0{}^i\mu_0)^2},$$

$$k_1{}^i=\left[3\left(1-\frac{3\pi^2}{32}g_i\omega_i\right)\right]^{1/2},$$

$$p_1{}^i=1/k_1{}^i,$$

$$\alpha_1{}^i=\frac{\frac{9}{16}\omega_i\mu_0F_0g_i(1-{\mu_0}^2)^{1/2}}{1-(k_1{}^i\mu_0)^2},$$

$$\beta_1{}^i=\mu_0\alpha_1{}^i.$$

Calculation of the four unknown constants $C_{00}^{\ i}$, $C_{01}^{\ i}$, $C_{10}^{\ i}$, and $C_{10}^{\ i}$ for each of N layer needs $4N$ equations. Four of these equations derive from the boundary conditions given below:

$$I^1(\tau = \tau_0,\ \mu,\ \phi) = 0, \tag{B5a}$$

$$I^N(\tau = \tau_N,\ \mu,\ \phi) = 0, \tag{B5b}$$

where μ is fixed to 2/3, while the remaining $4N - 4$ are determined by requiring that $I_{00}^{\ i}$, $I_{01}^{\ i}$, $I_{10}^{\ i}$, and $I_{11}^{\ i}$ are continuous:

$$\begin{cases} I_{00}^{\ i}(\tau_i) = I_{00}^{\ i+1}(\tau_i) \\ I_{01}^{\ i}(\tau_i) = I_{01}^{\ i+1}(\tau_1) \\ I_{10}^{\ i}(\tau_i) = I_{10}^{\ i+1}(\tau_i) \\ I_{11}^{\ i}(\tau_i) = I_{11}^{\ i+1}(\tau_1) \end{cases} \qquad i = 1,\ 2,\ \ldots,\ N-1. \tag{B6}$$

This work has been partially supported by the Italian Space Agency; by the Italian National Research Council through the National Project on Prevention from Hydro-Geological Disasters (GNDCI); and by the Italian Ministry of Education, University and Research. The GERM code is available from the authors upon request.

References

1. L. G. Henyey and J. L. Greenstein, "Diffuse radiation in the galaxy," Astrophys. J. **93,** 70–83 (1941).
2. W. M. Irvine, "Multiple scattering by large particles," Astrophys. J. **142,** 1563–1576 (1965).
3. T. Nakajima and M. Tanaka, "Algorithms for radiative intensity calculations in moderately thick atmospheres using a truncation approximation," J. Quant. Spectrosc. Radiat. Transfer **46,** 155–171 (1988).
4. R. Wu and J. A. Weinman, "Microwave radiances from precipitating clouds containing aspherical ice, combined phase, and liquid hydrometeors," J. Geophys. Res. **89,** 7170–7178 (1984).
5. C. Kummerow, "On the accuracy of the Eddington approximation for radiative transfer in the microwave frequencies," J. Geophys. Res. **98,** 2757–2765 (1993).
6. D. Tanrè, Y. J. Kaufman, M. Herman, and S. Mattoo, "Remote sensing of aerosol properties over oceans using the MODIS/EOS spectral radiances," J. Geophys. Res. **102,** 16971–16988 (1997).
7. F. S. Marzano, L. Roberti, S. Di Michele, A. Tassa, and A. Mugnai, "Modeling of apparent radar reflectivity due to convective clouds at attenuating wavelengths," Radio Sci. **38,** 1002 doi:10.1029/2002RS002613 (2003).
8. A. Ishimaru and R. L.-T. Cheung, "Multiple-scattering effect on radiometric determination of rain attenuation at millimeter-wavelengths," Radio Sci. **15,** 507–516 (1980).
9. F. S. Marzano, E. Fionda, and P. Ciotti, "Simulation of radiometric and attenuation measurements along earth-satellite links in the 10- to 50-GHz band through horizontally-finite convective raincells," Radio Sci. **34,** 841–858 (1999).
10. F. S. Marzano and L. Roberti, "Numerical investigation of intense rainfall effects on coherent and incoherent slant-path propagation at K band and above," IEEE Trans. Antennas Propag. **28,** 51–69 (2003).
11. S. Chandrasekhar, *Radiative Transfer* (Dover, 1960).
12. V. V. Sobolev, *A Treatise on Radiative Transfer* (Van Nostrand, 1962).
13. A. Ishimaru, *Wave Propagation and Scattering in Random Media* (IEEE Press, 1997).
14. K. N. Liou, *An Introduction to Atmospheric Radiation* (Academic, 1980).
15. P. Bauer, J. F. Mahfouf, W. S. Olson, F. S. Marzano, S. Di Michele, A. Tassa, and A. Mugnai, "Error analysis of TMI rainfall estimates over ocean for variational data assimilation," Q. J. R. Meteorol. Soc. **128,** 2129–2144 (2002).
16. K. Stamnes and R. A. Swanson, "A new look at the discrete ordinate method for radiative transfer calculations in anisotropically scattering atmospheres," J. Atmos. Sci. **38,** 387–399 (1981).
17. A. Gasiewskii, "Microwave radiative transfer in hydrometeors," in *Atmospheric Remote Sensing by Microwave Radiometry*, M. A. Jansen, ed. (Wiley, 1993), pp. 91–144.
18. W. J. Wiscombe, "The Delta-M method: rapid yet accurate radiative flux calculations for strongly asymmetric phase functions," J. Atmos. Sci. **34,** 1408–1422 (1977).
19. R. Davies, "Fast azimuthally dependent model of the reflection of solar radiation by plane-parallel clouds," Appl. Opt. **19,** 250–255 (1980).
20. J. A. Coakley and P. Chylek, "The two stream approximation in radiative transfer: including the angle of the incident radiation," J. Atmos. Sci. **32,** 409–418 (1974).
21. E. P. Shettle and J. A. Weinman, "The transfer of solar irradiance through inhomogeneous turbid atmospheres evaluated by Eddington's approximation," J. Atmos. Sci. **27,** 1048–1055 (1970).
22. J. H. Joseph, W. J. Wiscombe, and J. A. Weinman, "The Delta-Eddington approximation for radiative flux transfer," J. Atmos. Sci. **33,** 2452–2459 (1976).
23. M. D. King and H. Harshvardhan, "Comparative accuracy of selected multiple scattering approximations," J. Atmos. Sci. **43,** 784–801 (1986).
24. C. Levoni, E. Cattani, M. Cervino, R. Guzzi, and W. Di Nicolantonio, "Effectiveness of the MS-method for computation of the intensity field reflected by a multi-layer plane-parallel atmosphere," J. Quant. Spectrosc. Radiat. Transfer **69,** 635–650 (2001).
25. E. A. Smith, P. Bauer, F. S. Marzano, C. D. Kummerow, D. McKague, A. Mugnai, and G. Panegrossi, "Intercomparison of microwave radiative transfer models for precipitating clouds," IEEE Trans. Geosci. Remote Sens. **40,** 541–549 (2002).
26. W. Wiscombe and G. Grams, "The backscattered fraction in two-stream approximations," J. Atmos. Sci. **33,** 2440–2451 (1976).
27. W. E. Meador and W. R. Weaver, "Two-stream approximations to radiative transfer in planetary atmospheres: a unified description of existing methods and a new improvement," J. Atmos. Sci. **37,** 630–643 (1980).
28. X. Xiang, E. A. Smith, and C. G. Justus, "A rapid radiative transfer model for reflection of solar radiation," J. Atmos. Sci. **51,** 1978–1988 (1994).
29. W. J. Wiscombe and J. H. Joseph, "The range of validity of the Eddington approximation," Icarus **32,** 362–377 (1977).
30. K. Stamnes, S. C. Tsay, W. Wiscombe, and K. Jayaweera, "Numerically stable algorithm for discrete-ordinate-method radiative transfer in multiple scattering and emitting layered media," Appl. Opt. **27,** 2502–2509 (1988).
31. G. Ferrauto, F. S. Marzano, and G. Vulpiani, "Model-based sensitivity analysis of incoherent effects on microwave radar observations of precipitation media," in *Proceedings of the Third European Radar Meterology Conference and Hydrology* (Copernicus GmbH, 2004), pp. 201–208.
32. A. Tassa, S. Di Michele, A. Mugnai, F. S. Marzano, and P. Poiares Baptista, "Cloud-model based Bayesian technique for precipitation profile retrieval from TRMM Microwave Imager," Radio Sci. **38,** 8074–8086 (2003).